On comparing *in vivo* intracranial recordings in non-human primates to predictions of optimized transcranial electrical stimulation*

Abhishek Datta[$], Matthew R. Krause, Praveen K. Pilly[$], Jaehoon Choe, Theodoros P. Zanos, Chris Thomas, and Christopher C. Pack

Abstract— **Transcranial electrical stimulation (tES) can be optimized to achieve maximal current flow at desired brain regions. The aim of this study was to characterize electric field magnitudes generated by tES optimization and to compare them to experimentally induced values as determined by data from intracranial electrodes. Local field potentials were recorded from two monkeys with implanted multi-site intracranial Utah arrays during transcranial direct current stimulation (tDCS), and the neural effect predictions obtained from optimized electrode placement were assessed. Comparative data between the two sites of intracranial recordings during tDCS partially validated the predictions of our tES optimization algorithms.**

I. Introduction

Low intensity transcranial electrical stimulation (tES) involves the application of a wide range of waveforms which apply current (<5 mA) through scalp electrodes for modulating neural activity. tES includes direct current stimulation (tDCS), alternating current stimulation (tACS), pulsed current stimulation (tPCS), random noise stimulation (tRNS), and cranial electrotherapy stimulation (CES). Despite a multitude of animal and human studies, the current flow patterns induced by tES remain difficult to determine, even more so when anatomy is compromised [1]. Understanding of current flow patterns is therefore restricted to inferences from physiological and behavioral outcomes, which are often recorded post-stimulation. Computational models using finite-element-methods (FEM) are standard tools to determine current flow patterns in the brain and can be employed in not only analyzing experimental results retrospectively but also to prospectively plan stimulation parameters (electrode placements, size, amplitude, waveform, duration, etc.) and design optimal electrotherapies.

While the relative position and size of typical electrodes used in tDCS (~5x7 cm) can shape the outcome of stimulation, imaging and modeling studies suggest widespread current flow distributions. Using high-resolution FEM models and optimization algorithms, we predicted that High-Definition (HD) electrodes (~1 cm diameter) could be arranged in optimized montages to target specific structures of interest [2],[3]. Despite promising functional results from several clinical trials [4], it remains important to investigate the current delivery of these optimized approaches. We have previously compared patient-specific model predictions with functional MRI (fMRI) [5] and scalp potentials generated during tES [6]. Patient-specific models have also being used to compare direct physiological motor responses across subjects using the 4 x 1 montage (4x cathodes surrounding a single central anode) [7]. The 4 x 1 design however is just one representative HD montage while other montages maybe better suited to achieve optimal intensity or focality of stimulation [8].

The purpose of this study is to provide experimental and modeling evidence that partially support the predictions of optimized HD-tES. As part of a larger study to investigate the distributed neural bases of non-invasive stimulation at several levels of granularity, we studied the neural effects to various tES montages and parameters in two monkeys. In particular, we recorded single units and local field potential (LFP) signals using Utah arrays at two cortical sites (namely, prefrontal cortex (PFC) and inferotemporal cortex (ITC/TEO)). We built high resolution individualized monkey models, incorporating all the metallic implants on and in the head, and determined optimal stimulation montages targeting the implant locations. We then compared the effect sizes of modulation of the power of LFP signals in the theta (8-14 Hz), slow gamma (30-50 Hz), and fast gamma (50-150 Hz) bands from these optimal montages to the predicted electric field magnitudes to assess this approach.

II. Methods

A. Surgery and Implantation

We collected data from two adult male macaque monkeys (M and F). We began by collecting high-resolution T1 and T2-weighted MRIs (0.6-0.8 mm^3 voxels) from each animal. The animals were then implanted with a custom-made titanium headpost (Hybex Innovations, Anjou, Quebec),

* This work was supported by the Defense Advanced Research Projects Agency (DARPA) via contract number N66001-14-C-4066 (transcranial Stimulation to Improve Memory: tSTIM). The U.S. Government is authorized to reproduce and distribute reprints for Governmental purposes notwithstanding any copyright annotation thereon. The views and conclusions contained hereon are those of the authors and should not be interpreted as necessarily representing the official policies or endorsements, either expressed or implied, of DARPA or the U.S. Government.

A. Datta and C. Thomas are with Research and Development, Soterix Medical, Inc., New York, NY 10001, USA (tel: 888-990-8327; fax: 212-315-3232; e-mail: abhishek.datta@gmail.com).

M.R. Krause, T.P. Zanos, and C.C. Pack are with Montreal Neurological Institute, McGill University, Montreal, QC, H3A 2B4, Canada.

P.K. Pilly and J. Choe are with Information and Systems Sciences Laboratory, HRL Laboratories, LLC, Malibu, CA 90265 USA (tel: 310-317-5492; e-mail: pkpilly@hrl.com).

[$]corresponding authors

attached to the skull with 12-16 titanium screws (VOI, Inc.). Animals were allowed to recover for 8 weeks, then acclimatized to the laboratory environment and trained to perform the fixation task (see II.C below). Each animal was then rescanned with MRI fiducial markers attached to the headpost. We then performed a second surgery to implant the recording devices. Two iridium oxide (IrOx) microelectrode arrays (Utah Arrays; Blackrock Microsystems) were implanted in each animal – one in the temporal lobe visual area TEO/ITC and the other in prefrontal cortex (PFC) at the border of areas 8 and 9/46. These areas were identified on the anatomical scans and targeted using a frameless stereotaxic system (Brainsight, Rogue Research) with an accuracy of < 2mm. This system was used to record the location of the headpost legs, arrays, and other implanted devices. The arrays were implanted by first making a craniotomy over the target location, then implanting the array, and finally replacing the bone flap with metal straps. Surgeries were performed using standard sterile techniques and all animal experimentation was approved by the Animal Care Committee of the Montreal Neurological Institute and was conducted in compliance with regulations established by the Canadian Council of Animal Care.

B. Computational Workflow

We used the anatomical MRI scans from either monkey to first determine cortical current flow patterns due to transcranial electrical stimulation via computational models and then determined the most optimal scalp electrode positions maximizing electric field at intracranial locations (PFC and TEO/ITC). The steps for generating high-resolution, anatomically specific forward models for non-invasive transcranial stimulation are adapted from extensive prior work on computational modeling and optimization. These involve:

1) Segmentation of MR images into tissue categories (e.g. Skin, Skull, CSF, Gray Matter, White Matter, etc.) using a combination of automated and manual segmentation tools [9],[10]. This allows the delineation of tissues such that corresponding electrical conductivities can be assigned. The precision of the segmented tissues is pivotal for the generation of accurate 3D models in order to capture critical anatomical details (CSF architecture, gyri-sulci topography, etc.) that may influence current flow [11].

2) Modeling the exact physical geometry and properties of all surgical components- array, headpost, pedestal, bone flap, strap, etc. and precise placement within the segmented image data (for instance attaching the legs of the headpost to the skull mask). The precision of incorporating the exact geometry in the head volume, in the animal is critical to accurately model the current flow patterns. Stimulation electrodes are then positioned on the scalp using an automated script (for instance according to the 10-20 system). These locations form the candidate electrode set from which a much smaller number of physical electrodes (N electrodes) are selected (owing to restricted access due to various components of the implant).

3) Generation of accurate meshes (with a high quality factor) from the tissue/implant/electrode masks while preserving the resolution of anatomical data.

4) Resulting volumetric meshes are then imported into a finite element solver. At this step, resistivity is assigned to each mask (tissue, electrode, surgical components) and the boundary conditions imposed including the current applied to the N electrodes. Electrode Pz is designated as the reference and each remaining candidate electrode is energized one by one in succession solving the standard Laplacian equation using appropriate numerical solver and tolerance settings.

5) The N-1 bipolar configurations are then loaded into commercial modeling software (HDExplore, Soterix Medical) which allows visualization of cortical current flow from any electrode montage (designed using any of the available electrode locations combined in any fashion).

6) To determine the most optimal electrode montage targeting the implants, commercial optimization software (HDTargets, Soterix Medical) was used. HDTargets uses an optimization scheme (Linearly constrained minimum variance-LCMV) to determine linearly independent paths which are combined to yield a maximally focal or intense net electric field at target (see detailed optimization details in [3]).

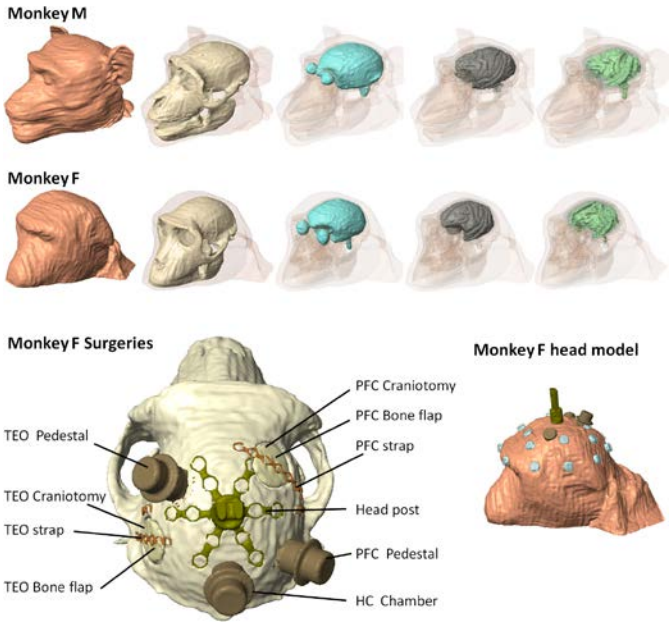

Figure 1. High-resolution individualized models. Top and Bottom: Segmentation masks of monkeys M and F (skin, skull, CSF, gray matter, white matter). Bottom left: Top view of the skull mask of monkey F revealing all the surgeries performed modeling exact experimental condition. Bottom right: Side view of the final head model of monkey F with stimulation electrodes (silver) positioned on the scalp.

7) Since HDTargets uses a 10-10 electrode scheme, for each one of the optimized predictions targeting the implants, corresponding electrode montages were chosen using a reduced sub-set of electrodes available for use in the monkey. For instance, for monkey M, 16 electrode locations were available. The candidate electrode montages are then screened using HDExplore to determine the most optimal solution targeting the implants (Table I). The optimized solutions are subsequently used in the experiments and the implant recordings compared with predicted EF intensities.

The following isotropic direct current electrical conductivities in (S m^{-1}) were assigned: scalp (0.465), skull

(0.01), CSF (1.65), gray matter (0.276), white matter (0.126), array ($1.89x10^7$), electrodes ($5.8x10^7$), paste (0.3). The metallic headpost, strap, and pedestal were all assigned a conductivity of $1.27x10^6$ S m^{-1}, while the bone flap was assigned the conductivity of skull.

TABLE I. OPTIMAL MONKEY-SPECIFIC STIMULATION MONTAGES FOR THE TWO OPTIMIZATION CONSTRAINTS AND THE TWO TARGETS.

Monkey	Optimization constraint	PFC	TEO/ITC
M	Max Intensity	Fp2=+2 mA O2=-2 mA	Fp1=+2 mA P7=-2 mA
	Max Focality	Fp2=+1.23 mA F4=+0.77 mA F3=-0.81 mA C3=-0.38 mA T4=-0.81 mA	T5=+1.36 mA C3=+0.64 mA F7=-1.06 mA T3=-0.48 mA O2=-0.45 mA
F	Max Intensity	F4= +2 mA P7= -2 mA	P3=+2 mA Fp1=-2 mA
	Max Focality	F4=+2 mA Fp1=-0.74 mA Fp2=-0.61 mA F8=-0.65 mA	P3=2 mA C4=-0.16 mA P4=-1.06 mA F7=-0.78 mA

C. Transcranial Stimulation and Recording

tDCS was performed with various montages (see Table I) using a commercially available tES system intended for human subjects (StarStim; Neuroelectrics). The 1 cm radius Ag/AgCl electrodes were coated with conductive paste and attached to the scalp using a silicon elastomer (Kwik-Sil, World Precision Instruments). Electrode impedance was always below 10 KΩ and typically less than 2 KΩ.

We recorded wideband signals from both arrays simultaneously using a Neural Interface Processor (Ripple, Salt Lake City, Utah). The signal was sampled at 30,000 Hz and band-pass filtered between 0.3 and 7500 Hz during acquisition. The data was subsequently processed offline to extract single-unit spiking activity and the local field potential. Single units were detected and sorted using a wavelet-based clustering approach [12], and manually reviewed for quality. We estimated the local field potential by low-pass filtering the LFP to 500 Hz; power line artifacts and contamination from nearby spikes were removed using a Bayesian approach [13].

Animals were trained to fixate a small black dot presented in the center of a grey screen while their eyes were tracked with an infrared eye tracking system (Eyelink II; SR Research). If the animal maintained fixation within 1˚ for 1-2 seconds, it received a small liquid reward; eye movements during this period aborted and restarted the timer. The delay was randomly selected from a truncated exponential distribution on each trial; this distribution has a flat hazard rate and therefore reduces the animals' ability to anticipate rewards. Recording, stimulation, and the behavioral paradigm were controlled by custom software written in C and MATLAB. Stimulation was applied for 5 min while the monkeys maintained fixation.

D. LFP Analysis

We built a data analysis pipeline to statistically assess dynamic changes in LFP spectral content during stimulation and post-stimulation for various non-invasive stimulation parameters. In particular, this pipeline uses resampling statistics and two-sample Kolmogorov-Smirnov goodness-of-fit hypothesis test to measure shifts from baseline. It outputs *p*-value as a function of time during stimulation and post-stimulation, and also computes additive/multiplicative modulation index as well as the time-to-return to baseline during stimulation and post-stimulation. We analyzed the LFP power in the theta (8-14 Hz), slow gamma (30-50 Hz), and fast gamma (50-150 Hz) bands among other neural metrics, in order to test the predictions of the different tES montages (max intensity and max focality) as computed above. Data corrupted due to stimulation onset and offset-related artifacts were excluded from the data analysis. For transcranial current stimulation (tES), data collected within 8 s following stimulation onset and prior to and following offset were ignored.

In order to determine the duration of effect, we utilized a novel analysis method that varied the sample window size such that we compare a limited temporal window of the stimulation/post-stimulation period with the null distribution. As a result, we were able to determine the precise time windows in which the modulation is statistically significant, and can therefore derive the time at which the LFP returns to statistically insignificant levels; we call this time Return-to-Baseline (R2B).

III. RESULTS

Figures 2 and 3 shows the modulation across 5 trials in the LFP spectral content at five randomly chosen channels in each Utah array during stimulation in response to 5 min of max intensity and max focality tDCS montages, respectively, that were targeted at the TEO/ITC array location. The random choice of five channels per array was done merely for convenience, and was checked to not affect the generality of our conclusions from the analyses. For each channel, the period over which the shift from baseline (2 min duration immediately prior to stimulation onset) stayed statistically significant during stimulation was calculated. The top row in either figure shows the temporal average of the magnitude of the modulation effect, as a proportion of the baseline, over these periods. And the bottom row in either figure shows the corresponding Return-to-Baseline times. Consistent with predictions (see Table II), we can see that in response to max intensity tDCS montage targeted at TEO/ITC, the greatest modulation is seen in TEO/ITC compared to PFC for the LFP theta band power. We also note that the modulation in the gamma bands doesn't seem to differ between the two areas.

TABLE II. PREDICTED INDUCED ELECTRIC FIELD MAGNITUDES (V/m) FOR EACH OPTIMAL ELECTRODE MONTAGE TESTED.

Monkey	Target	Optimization	PFC	TEO/ITC
M	PFC	Intensity	0.68	0.06
	PFC	Focality	0.47	0.12
	TEO	Intensity	0.29	0.23
	TEO	Focality	0.04	0.19
F	PFC	Intensity	0.42	0.34

Further, consistent with the weaker predicted EF values for the max focality compared to the max intensity montage, we can see that the observed modulations in the LFP theta band are weaker for the max focality montage (compare the top rows in Figures 2 and 3).

There are also deviations between the model predictions and the *in vivo* neural effects. For instance, the modulation in PFC is predicted to be slightly stronger than in TEO for the TEO max intensity montage, but the data in monkey M has the opposite trend (see Figure 2). While the congruencies between model predictions and the neural data

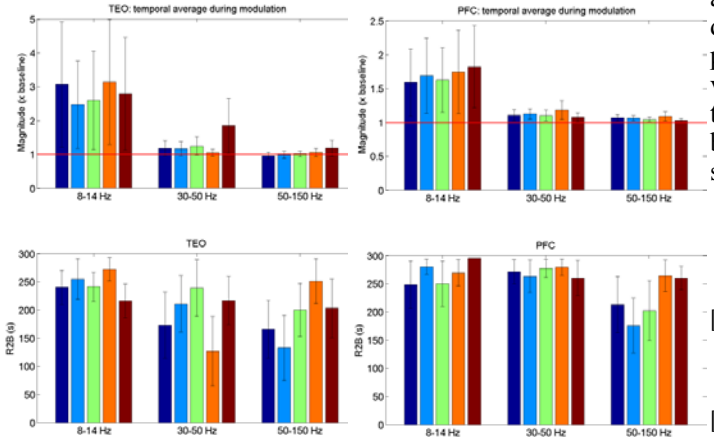

Figure 2. LFP effects in response to 5 min max intensity tDCS TEO montage for monkey M. Modulation effect sizes and durations of statistically significant modulation during the stimulation at five randomly chosen channels in each of the Utah arrays implanted in TEO and PFC, for the LFP power in the theta, slow gamma, and fast gamma bands. Error bars correspond to standard error of mean across 5 trials. R2B: Return-to-Baseline duration.

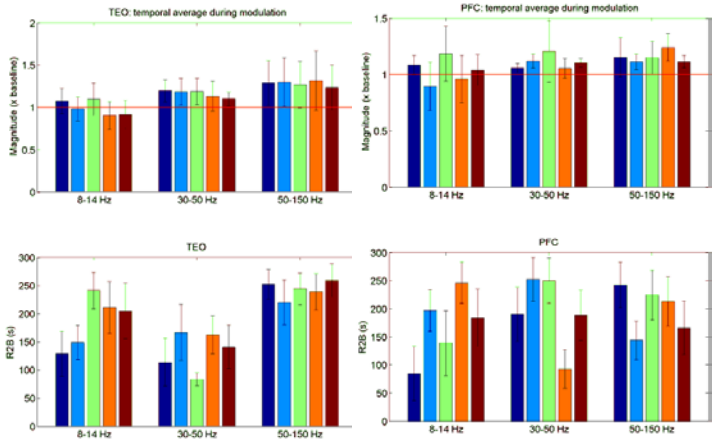

Figure 3. LFP effects in resposne to 5 min max focality tDCS TEO montage for monkey M. Modulation effect sizes and durations of statistically significant modulation during stimulation at five randomly chosen channels in each of the Utah arrays implanted in TEO and PFC, for the LFP power in the theta, slow gamma, and fast gamma bands. Error bars correspond to standard error of mean across 5 trials. R2B: Return-to-Baseline duration.

provide partial validation of our particular stimulation optimization methodology, the incongruences that do exist point to the need for further advancing our modeling approach. This includes accounting for various structural and functional connections between different brain areas and presumably monkey-specific tissue conductivites.

DISCUSSION

This study is motivated by the aim to characterize current flow maps due to optimized tES as part of a larger study to investigate distributed neural bases of non-invasive stimulation using *in vivo* intracranial array recordings in primates. Our experimental measurements provide partial agreement to the optimized model predictions but do not directly validate them. Still, the consistency of modeling predictions with experimental data provides support to various optimization approaches. More work will be needed to incorporate the structural and functional interactions between various brain areas in a living brain to fully optimize stimulation montages for targeting particular brain sites.

REFERENCES

[1] A. Datta, J.M. Baker, M. Bikson, and J. Fridriksson, "Individualized model predicts brain current flow during transcranial direct-current stimulation treatment in responsive stroke patient," Brain Stimul. vol 4, pp. 169-74,Jul 2011

[2] A. Datta, V. Bansal, J. Diaz, J. Patel, D. Reato, and M. Bikson, "Gyri-precise head model of transcranial direct current stimulation: improved spatial focality using a ring electrode versus conventional rectangular pad," Brain Stimul 2009 Oct;2(4):201-7, 207.e1.

[3] J.P. Dmochowski, A. Datta, M. Bikson, Y. Su, and L.C. Parra, "Optimized multi-electrode stimulation increases focality and intensity at target," *J Neural Eng.* vol 8, Aug 2011

[4] L. Castillo-Saavedra, N. Gebodh, M. Bikson, C. Diaz-Cruz, R. Brandao, L. Coutinho et al., "Clinicall effective treatment of Fibromyalgia pain with high-definition transcranial direct current stimulation: phase II open-label dose optimization," *J Pain*, vol 17, pp.14-26, Jan 2016

[5] M.A. Halko, A. Datta, E.B. Plow, J. Scaturro, M. Bikson, L.B. Merabet, "Neuroplastic changes following rehabilitative training correlate with regional electric field induced with tDCS," *Neuroimage*, vol 57, pp. 885-91, Aug 2011

[6] A. Datta, X. Zhou, Y. Su, L.C. Parra, and M. Bikson, "Validation of finite element model of transcranial electrical stimulation using scalp potentials," *J Neural Eng.* vol 10, Jun 2013

[7] D. Edwards, et al., "Physiological and modeling evidence for focal transcranial electrical stimulation in humans: a basis for high-definition tDCS," *Neuroimage* vol 1, pp.266-75, Jul 2013

[8] J. Richardson, A. Datta, J. Dmochowski, L.C. Parra, J. Fridriksson, "Feasibility of using high-definition transcranial direct current stimulation (HD-tDCS) to enhance treatment outcomes in persons with aphasia," *NeuroRehabilitation*, vol 36, pp. 115-26, 2015

[9] A. Datta, D. Truong, P. Minhas, L.C. Parra, M. Bikson, "Inter-individual variation during transcranial direct current stimulation and normalization of dose using MRI-derived computational models," *Front Psychiatry*, vol 91, Oct 2012

[10] Y. Huang, J.P. Dmochowski, Y. Su, A. Datta, C. Rorden, L.C. Parra, "Automated MRI segmentation for individualized modeling of current flow in the human head," *J Neural Eng.* vol 10, Dec 2013

[11] M. Bikson and A. Datta, "Guidelines for precise and accurate computational models of tDCS," vol 5, pp.430-1, Jul 2012

[12] R.Q. Quiroga, Z. Nadasdy, Y. Ben-Shaul, "Unsupervised spike detection and sorting with wavelets and superparamagnetic clustering," *Neural Comput.* vol 16, pp 1661-87 Aug 2004

[13] T.P. Zanos, P.J. Mineault, C.C. Pack, "Removal of spurious correlations between spikes and local field potentials," *J Neurophysiol.* vol 105, pp. 474-86 Jan 2011